Structure Elucidation | *Hot Paper*

New Noncentrosymmetric Tetrel Pnictides Composed of Square-Planar Gold(I) with Peculiar Bonding

Shannon J. Lee,[a, b] Juyeon Won,[a, b] Lin-Lin Wang,[b] Dapeng Jing,[b, c] Colin P. Harmer,[a, b] Justin Mark,[a, b] Georgiy Akopov,[a, b] and Kirill Kovnir*[a, b]

Abstract: Three novel isostructural equiatomic gold tetrel pnictides, AuSiAs, AuGeP, and AuGeAs, were synthesized and characterized. These phases crystallize in the noncentrosymmetric (NCS) monoclinic space group *Cc* (no. 9), featuring square-planar Au within *cis*-[$AuTt_2Pn_2$] units (Tt = tetrel, Si, Ge; Pn = pnictogen, P, As). This is in drastic contrast to the structure of previously reported AuSiP, which exhibits typical linear coordination of Au with Si and P. Chemical bonding analysis through the electron localization function suggests covalent two-center two-electron Tt–Pn bonds, and three-center Au–Tt–Au and Au–Pn–Au bonds with 1.6 e^- per bond. X-ray photoelectron spectroscopy studies support the covalent and nonionic nature of Au–Pn and Au–Tt bonds. The title materials were found to be *n*-type narrow-gap semiconductors or semimetals, with nearly temperature-independent electrical resistivities and low thermal conductivities. A combination of the semimetallic properties with tunable NCS structure provides opportunities for the development of materials based on gold tetrel pnictides.

Introduction

The discovery of novel noncentrosymmetric (NCS) materials is a necessary and crucial component to develop technologies such as superconductors, topological materials, and nonlinear optical materials.[1] The recent discovery of tetrel pnictides $Ba_2Si_3P_6$, $MnSiP_2$, $ZnGeP_2$, and $MgSiAs_2$, with a remarkable balance between the laser damage threshold and a second-harmonic generation signal,[2–5] sparked the question of whether other metal tetrel pnictides may also exhibit NCS structures. In general, inorganic NCS compounds are quite rare in intermetallic compounds (≈10%).[6] However, there are 36 ternary phases reported for transition metals (M = Ti–Cu, Zr–Ag, and Hf–Au) in the M–Si–P systems, 70% of which are NCS. Moreover, for the phases with M content lower than 50 at%, that is, M/(Si + P) < 1, the abundance of NCS structures is extremely high, 95%.[6] The presence of two nonmetal elements, Si and P, which, through both M–Si and M–P bonds, can coordinate transition metals to form NCS local fragments that are linked through strong covalent Si–P bonds, allows for structures that lack inversion symmetry. Although ternary silicon phosphides are well explored, other tetrel pnictide systems (M–Si–As, M–Ge–P, and M–Ge–As) are much less studied. Herein, we specifically investigate the novel gold tetrel pnictides AuSiAs, AuGeP, and AuGeAs.

Traditionally, metal pnictides are described as having polar covalent bonds between an electropositive metal atom and electronegative P or As atoms. This is not true for Au, which is unique, as the most electronegative transition metal.[7] On the Pauling scale of electronegativity, Au has the largest value, 2.5, compared with those of Si (1.9), Ge (2.0), P (2.2), and As (2.2).[8] Additionally, a lanthanide contraction and relativistic effects for the 6s electrons make Au chemistry particularly interesting.[9–13] The combination of Au with Si and P results in a unique NCS crystal structure of AuSiP not found among other transition-metal tetrel pnictides.[14] In AuSiP, Si and P form puckered ordered hexagonal layers, connected by linearly coordinated Au atoms (Figure 1). A different centrosymmetric structure, NiP_2 type,[15–17] was proposed for AuGeAs based on thin-film studies.[18] Such structural determination is challenging because of the inability to distinguish Ge from As, due to similarities in their X-ray scattering factors. Herein, we present the discovery of three unique gold tetrel pnictides, AuSiAs, AuGeP, and AuGeAs. We report the synthesis, crystal structures, chemical bonding, and properties of the three NCS materials. Notably, the title gold tetrel pnictides exhibit square-planar (2 tetrel (Tt) and 2 pnictogen (Pn)) Au coordination, with two- and three-center bonding interactions.

[a] S. J. Lee, J. Won, C. P. Harmer, Dr. J. Mark, Dr. G. Akopov, Prof. K. Kovnir
Department of Chemistry, Iowa State University
Ames, IA 50011 (USA)
E-mail: kovnir@iastate.edu

[b] S. J. Lee, J. Won, Dr. L.-L. Wang, Dr. D. Jing, C. P. Harmer, Dr. J. Mark, Dr. G. Akopov, Prof. K. Kovnir
U.S. Department of Energy, Ames Laboratory
Ames, IA 50011 (USA)

[c] Dr. D. Jing
Materials Analysis and Research Laboratory
Iowa State University, Ames, IA 50011 (USA)

Supporting information and the ORCID identification number(s) for the author(s) of this article can be found under: https://doi.org/10.1002/chem.202005312.

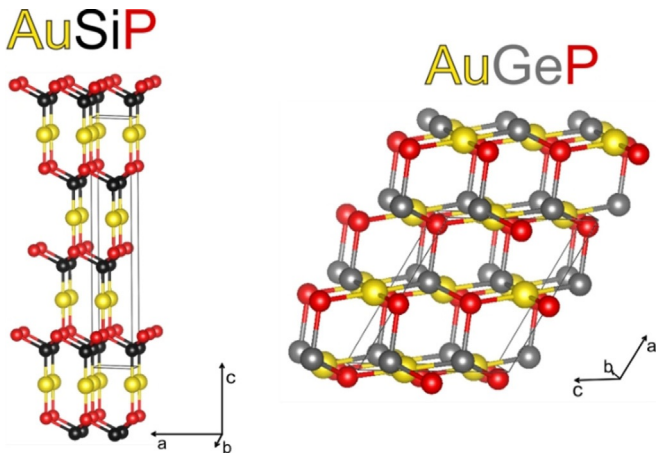

Figure 1. A comparison of AuSiP and AuGeP (isostructural to AuSiAs and AuGeAs) crystal structures with unit cells outlined in gray. Au: yellow, Si: black, Ge: gray, P: red.

Results and Discussion

Synthesis and thermal stability

AuSiP has a unique crystal structure (Figure 1) that exhibits a linear Au coordination (1 Si + 1 P). However, if heavier tetrel or pnictogen elements are used, such as in AuSiAs, AuGeP, and AuGeAs, a different NCS structure emerges. This structure is an ordered version of the monoclinic NiP_2 structure.[15] The NCS nature stems from the *cis*-[$AuTt_2Pn_2$] (Tt = Si, Ge; Pn = P, As) square-planar coordination (Figure 2b). In this *cis*-planar geometry, no inversion center exists.

Structurally different AuSiP and the remaining AuTtPn (Tt = Si, Ge; Pn = P, As) derivatives required vastly different synthetic procedures. The synthesis of AuSiP, as previously reported,[14] requires high-temperature annealing, specific slow cooling, and air quenching to make a single-phase sample. The optimized syntheses of AuSiAs, AuGeP, and AuGeAs reported here were shortened to a single step and used lower temperature annealing without the need for an extra quenching step to obtain single-phase products. Synthetic details may be found in the Supporting Information. Differential scanning calorimetry (DSC; Figure S1 in the Supporting Information) shows decomposition/melting events at 963, 709, 684, and 604 °C for AuSiP, AuSiAs, AuGeP, and AuGeAs, respectively. Post-DSC samples contained significant amounts of elemental Au and tetrel. Comparing DSC decomposition temperatures, a general trend is observed for decreasing thermal stabilities if Si is replaced with Ge or P with As. The thermal decomposition pathway of AuGeP was confirmed by in situ powder XRD data collected at 17-BM at the Advanced Photon Source at the Argonne National Laboratory (Figures S2 and S3 in the Supporting Information). The optimized synthetic conditions correspond to reaction at temperatures slightly below the decomposition temperatures: AuSiP (900 °C), AuSiAs (600 °C), AuGeP (600 °C), and AuGeAs (575 °C). This ensured sufficient reactivity of the starting materials and prevented side-phase formation upon melting/decomposition of the target phase. Nearly phase-pure samples of all three novel phases were obtained through these optimized synthetic methods (Figure S4 in the Supporting Information).

Crystal structure determination

AuGeAs was originally reported in the centrosymmetric space group of *C*2/*c* (no. 15),[18] with one Au site at position 4*c* and one mixed occupancy site of 50% Ge and 50% As at general position 8*f*. However, similar scattering factors for Ge and As make establishment of the correct space group challenging.[19,20] To find the true space group, high-resolution single-

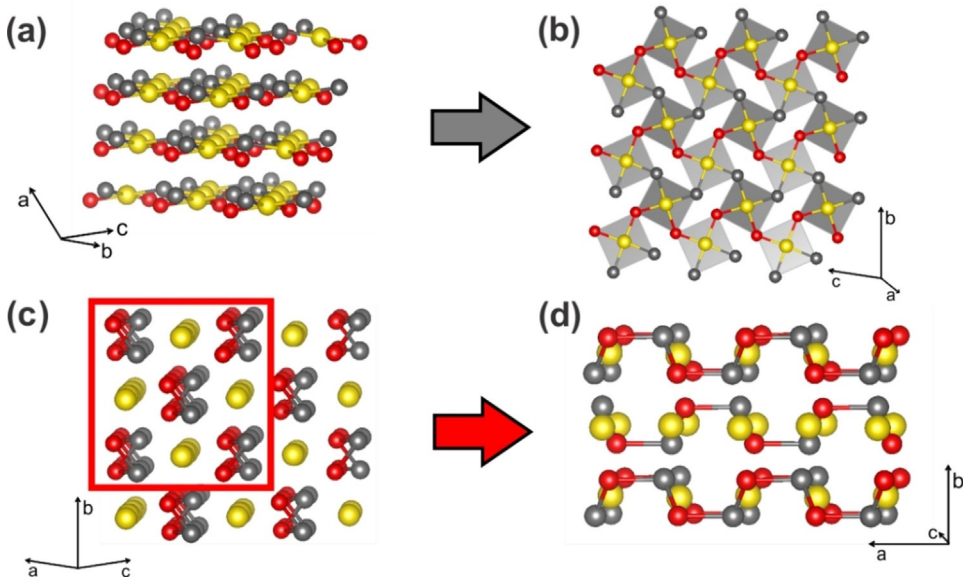

Figure 2. Crystal structure of AuGeP emphasizing the layers of square-planar *cis*-[$AuGe_2P_2$] coordination with a) stacking of Au–Ge–P layers, b) top view of one layer with square-planar units highlighted in gray, c) Ge–P chains throughout the structure, and d) side view of the Ge–P chains. Au: yellow, Ge: gray, P: red.

crystal XRD datasets were collected ($\sin\theta_{max}/\lambda = 0.90$ Å^{-1}) and solved in both space groups, *Cc* and *C*2/*c*. Initial refinement of our AuGeAs single-crystal diffraction dataset in the reported *C*2/*c* space group resulted in an R_1 value of 0.019 and an unusually low goodness-of-fit value of 0.85. This solution showed a fully occupied Au site and a mixed occupancy of the 8*f* Ge/As site, with site occupancy factors of 0.6(1)/0.4, respectively. Despite the mixed occupancy of Ge and As being reported,[19] in most cases, Ge and As prefer to occupy separate atomic sites.[20–25] In the NCS space group *Cc* (no. 9), there are three fully occupied 4*a* sites (1 Au, 1 Ge, 1 As). This refinement resulted in a lower R_1 value of 0.016, a reasonable goodness-of-fit of 0.99, and a Flack parameter of 0.11(3). The crystal structures of AuSiAs and AuGeP described below also crystallize in the monoclinic *Cc* space group, providing an additional argument for AuGeAs to be NCS.

For AuSiAs, the structural refinement was much more conclusive, with the advantage of a higher quality crystal and differing X-ray scattering factors of Si and As. AuSiAs solved in the *Cc* space group had three fully occupied 4*a* sites (1 Au, 1 Si, and 1 As). The solution resulted in a low R_1 value of 0.022 and a low Flack parameter of 0.01(2). AuGeP was found to be isostructural to AuSiAs; the difference was that, whereas the Au site was fully occupied, a minor (≈7%) mixing of Ge and P was observed in the two remaining sites: $Ge_{0.929(4)}P_{0.071}$ and $Ge_{0.076}P_{0.934(4)}$. This refinement resulted in an R_1 value of 0.011 and a Flack parameter of 0.08(1). Further details are given in the Supporting Information. We hypothesize that the degree of site mixing may be attributed to the closer electronegativity of Ge and P, as opposed to the larger difference of Si and As. The Ge/P mixing was reproducibly found in several crystals of AuGeP selected from different synthetic batches. Due to similar scattering factors of Ge and As, we cannot exclude potential partial mixing of Ge and As in the same sites in the crystal structure of AuGeAs; however, our diffraction experiments suggest that *Cc* is the correct space group for this family of gold tetrel pnictides. Based on current XRD data, the possibility of partial Ge/As mixing, as observed for AuGeP, cannot be ruled out. Neutron diffraction or resonant XRD experiments are required to verify or disprove Ge/As mixing in the structure of AuGeAs.

Crystal structures

The AuGeP crystal structure can be described as layers of corner-sharing *cis*-[$AuGe_2P_2$] square-planar units. Although square-planar coordination of Au^{III} has been commonly reported for molecular compounds, in extended solids square-planar units are typically dominated by halides, oxides, and chalcogenides, [AuX_4] (X = I, O, S, Se).[26–29] A rare example of the pnictide square-planar unit is the flat Au_3As_8 layer composed of [$AuAs_4$] units connected through As–As bonds in the structure of $Nd_{10}Au_3As_8O_{10}$.[30] Among the reported Au tetrel pnictide fragments, to the best of our knowledge, AuTtPn compounds of 1:1:1 composition are the first example of a solid-state network composed of square-planar $AuTt_2Pn_2$ units.[31] The layers are connected in the stacking direction through additional Ge–P bonds (Figure 1). The tetrel pnictide sublattice consists of spiral-like Ge–P chains of alternating Ge and P atoms propagating along the [101] direction (Figure 2). In the case of the previously reported structure of *m*-NiP_2, Ni is coordinated by a square of four P atoms and the covalently bonded chains are composed solely of P atoms. In AuGeP, there are three distinct crystallographic sites: a fully occupied Au site and two mixed Ge/P sites. One of these sites is mostly occupied by Ge (≈93%), whereas the other is mostly occupied by P (≈93%). The Au–Ge distance of 2.47 Å in this structure is shorter than that of typical Au–Ge bonds, but are similar to those found in a few structures: 2.41 ($K_4Au_7Ge_2$)[32] and 2.51 Å ($Ba_8Au_6Ge_{40}$).[33] Au–P and Ge–P distances of 2.40 and 2.34–2.36 Å, respectively, are comparable to the corresponding distances of 2.34 (Au_2P_3),[34] 2.37 ($BaAu_2P_4$),[35] 2.32–2.58 ($Ba_8Au_{16}P_{30}$),[36] and 2.34–2.38 Å (GeP).[37] The Au–Au distance in AuGeP is 3.37 Å, which is too long to be considered a covalent bond, but is a reasonable distance for aurophilic interactions, as observed in the gold iodide structure.[38,39] The Au atoms form almost linear chains (∢Au-Au-Au = 176.9°). The nature of the Au–Au interactions were investigated further by chemical bonding analysis in direct space (see below).

Both AuSiAs and AuGeAs are isostructural to AuGeP. The Au–Si distance of 2.40 Å is comparable to distances of 2.36 (AuSiP)[14] and 2.43 Å ($CaAu_2Si_2$),[40] whereas the Au–Ge bond of 2.48 Å is similar to that of AuGeP. The Si–As (2.36–2.38 Å) and Ge–As (2.45–2.46 Å) bond lengths found in these phases are similar to those of the SiAs (2.36–2.42 Å)[41] and GeAs (2.46–2.47 Å)[21,42] binary compounds. Similar Au–Au distances (as in AuGeP) are observed in AuSiAs and AuGeAs of 3.42 and 3.46 Å, respectively, both phases with nearly linear Au chains (∢Au-Au-Au = 176.2 and 179.7°). The relevant crystallographic data are summarized in Table S1 in the Supporting Information.

Coordination numbers (CNs) two and three in linear and trigonal planar/pyramidal geometries are common for Au in pnictides or silicides, whereas a CN of four is less common and typically corresponds to tetrahedral Au (Table 1). Square-planar arrangements with Au^{III} coordination are observed in some chalcogenides and oxides in extended solids.[26–29] However, nonbridged square-planar-coordinated Au in the +1 oxidation state is much less common in extended solids.[30]

Quantum chemical calculations

Electronic band structure and density of states (DOS) have been calculated for the four Au–Tt–Pn compounds in the Perdew–Burke–Ernzerhof (PBE)[43] exchange-correlation functional with spin-orbit coupling (SOC) included. AuGeP is used as an example here; the remaining band structures and DOS plots are shown in Figure S5 in the Supporting Information. From the band structure shown in Figure 3a, AuGeP has an indirect band gap of 0.56 eV. The valence-band maximum is near the Γ point, whereas the conduction-band minimum is away from the zone center and along the *H*–*Z* direction. The small splitting of bands arises from the absence of inversion symmetry, which lifts the spin degeneracy in SOC calculations for

Table 1. Examples of various types of Au coordination in several tetrel- or pnictogen-containing phases.

Composition	Au–(Tt/Pn) distance [Å]	Au CN	Coordination geometry
AuSiP	2.33	2	linear
$BaAu_3Si$	2.44–2.86	2	linear
Au_2P_3	2.33–2.34	2	linear
$BaAu_2P_4$	2.36	2	linear
BaAuAs	2.62	3	trigonal planar
CaAuAs	2.53	3	trigonal planar
ThAuSi	2.46	3	trigonal Planar
Ce_2AuP_3	2.46–2.52	3	tetrahedral
$CaAu_2Si_2$	2.43	4	tetrahedral
$Ba_8Au_{16}P_{30}$	2.34–2.58	4	tetrahedral
$Nd_{10}Au_3As_8O_{10}$	2.54–2.59	4	square planar
molecular example			
$C_{20}H_{32}AuP_2Si_2$ (bis(silyl)gold(III) complex)	2.38–2.44	4	square planar

these NCS structures. DOS has been projected on atomic orbitals for AuGeP in Figure 3b. Most of the Au 5d band spans from −7 to −3 eV, whereas there is also a shoulder from −3 to 0 eV. In both regions, the Au 5d orbital has a strong resonance; thus, hybridization with Ge 4p and P 3p orbitals is present. In contrast to the Ge 4s band located at around −12 eV and P 3s at around −9 eV, the Au 6s band is much broader and spans most of the valence-band region. Due to strong relativistic effects, the Au 6s orbital is contracted toward the nuclei and pushes the Au 5d orbital to higher energy to strongly hybridize with Tt p and Pn p orbitals. The contracted Au 6s orbital implies higher electronegativity or, equivalently, a larger work function, making it more difficult for Au to lose electrons compared with Ag or Cu. This explains the very small presence of the Au 6s orbital in the conduction band in Figure 3b. Thus, the bonding in these compounds is mostly of covalent character.

All four gold tetrel pnictide phases are predicted to be semiconductors with decreasing band gaps of 1.4 (AuSiP), 0.6 (AuGeP), 0.4 (AuSiAs), and 0.2 eV (AuGeAs). This trend is as expected, with the heavier elements having better orbital overlap, and therefore, having smaller band gaps. These calculations were conducted by using idealized structural models that did not include mixing of the tetrel and pnictogen sites (i.e., fully occupied sites with Tt or Pn). This may affect the exact value of the band gap for the materials, for which the actual structure has such mixing involved. An additional calculation was conducted for a hypothetical structure of AuGeP, in which partial exchange of Ge and P atoms resulted in the formation of –Ge–Ge–P–P– chains instead of –Ge–P–Ge–P– ones. Band-structure calculations reveal this hypothetical AuGeP structure to be a narrow band gap semiconductor (Figure S6 in the Supporting Information), showing that Ge/P mixing is not expected to drastically change the electronic structure of the material.

To firmly establish the trend in band gaps across the AuTtPn series, we have also used the modified Becke–Johnson (mBJ) exchange-correlation potentials, which is a metageneralized gradient approximation (meta-GGA) known for correcting an underestimated band gap. Relative to the corresponding band structure with PBE + SOC, the valence and conduction bands of the four compounds with mBJ + SOC are moved lower and higher in energy, respectively (Figure S7 in the Supporting Information). The resulting band gaps are slightly larger by 0.2–0.3 eV (Table S2 in the Supporting Information) for all compounds, preserving the overall trend of the band gap values: AuGeAs < AuSiAs < AuGeP < AuSiP.

For *m*-NiP_2 with 1D P chains, the formal oxidation states can be assigned as $Ni^{2+}(P^{1-})_2$, leading to expected d^8 electronic state for square-planar coordination. A consideration of the formal oxidation states in AuGeP, assuming Ge and P realize an electron octet and Au is a cation, results in an assignment of $Au^{3+}Ge^{2-}P^{1-}$. Both Ge and P form two covalent bonds to each other, and thus, each requires six electrons to form two bonds and two electron lone pairs. Square-planar coordination is not uncommon for d^8 metals in molecular compounds, including Au^{III} complexes (Table 1). In contrast to this assignment, Au is the most electronegative element in the AuTtPn family of materials. To clarify the chemical bonding picture, computational analysis was performed.

Based on the electron localization function (ELF) analysis (Figure 4), the covalent bonds are formed between tetrel and pnictogen in both AuGeP and AuSiAs. There are also bonding attractors corresponding to Au–{P, Si, Ge, As} bonds. The non-

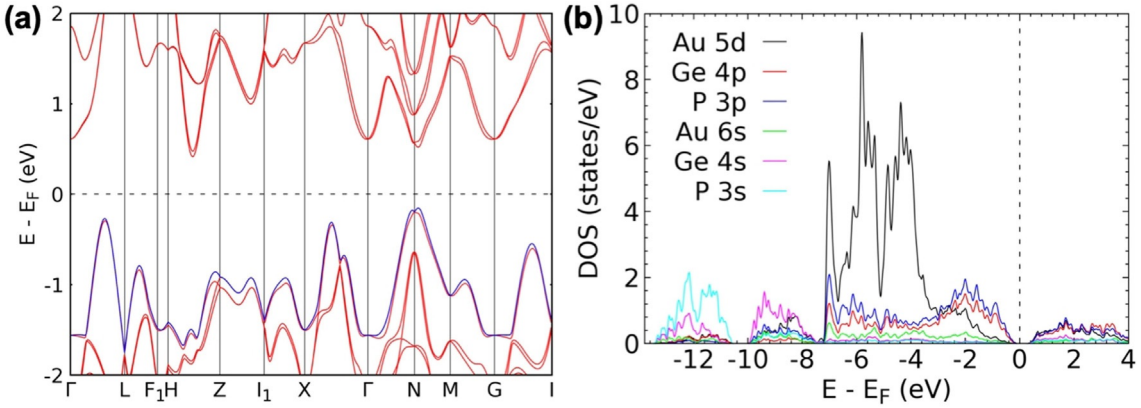

Figure 3. a) Electronic band structure and b) projected DOS for AuGeP calculated with PBE + SOC. The top valence band in a) is shown in blue.

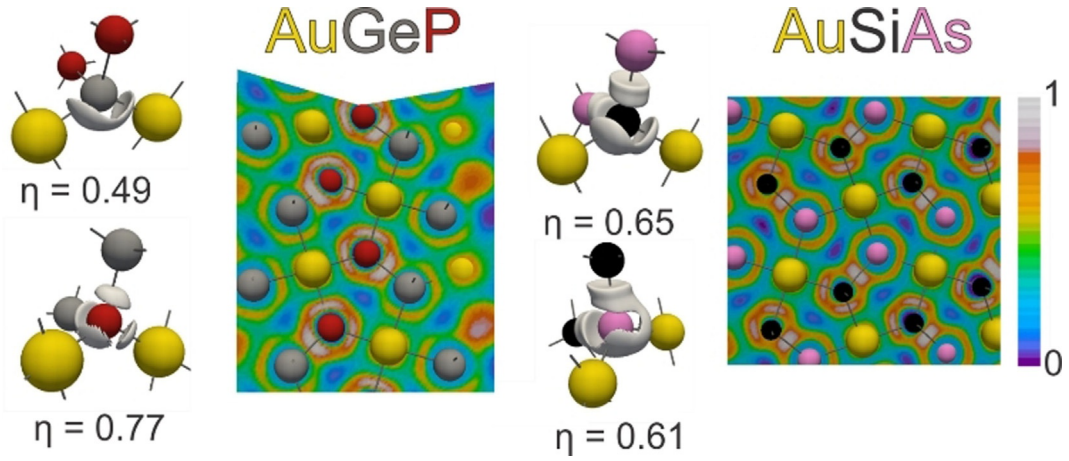

Figure 4. ELF isosurfaces with various η values, emphasizing tetrahedral coordination around Ge, P, Si, and As, and slices of the ELF of AuGeP and AuSiAs. Au: yellow, Si: black, Ge: gray, P: red, As: pink.

metal–nonmetal interactions are more structured than the Au–Tt and Au–Pn interactions. To further analyze these bonds, a basin analysis through the Bader approach was conducted (Figure 5 and Figure S8 in the Supporting Information). With AuGeP as a specific example, disynaptic basins (basins touching cores of two atoms) for Ge–P bonds with an electron density of 2 e^- correspond to covalent two-center two-electron bonds. Basins corresponding to Au–Ge (1.64 e^-) and Au–P (1.60 e^-) interactions have lower electron density. Moreover, Au–Ge and Au–P basins are not entirely disynaptic because they touch the cores of two gold atoms, corresponding to three-center bonds (highlighted in Figure 5c and Figure S8c in the Supporting Information). The Au–Au distances in the nearly linear chains (ranging from 3.37–3.46 Å) are within a reasonable distance for weak aurophilic interactions.[38,39] The basin analysis shows that the Au core basin contains 78 e^-, suggesting the Au^+ d^{10} configuration. Overall, Au is therefore involved in two two-center bonds (Au–Ge and Au–P) with Ge and P atoms from its own $AuGe_2P_2$ unit, two three-center bonds (Au–Au–Ge and Au–Au–P) with Ge and P atoms from its own $AuGe_2P_2$ unit, and two three-center bonds (Au–Au–Ge and Au–Au–P) with Ge and P atoms from the $AuGe_2P_2$ units above and below. Notably, every Ge or P atom is involved in three two-center bonds and one three-center interaction (Figure 5d).

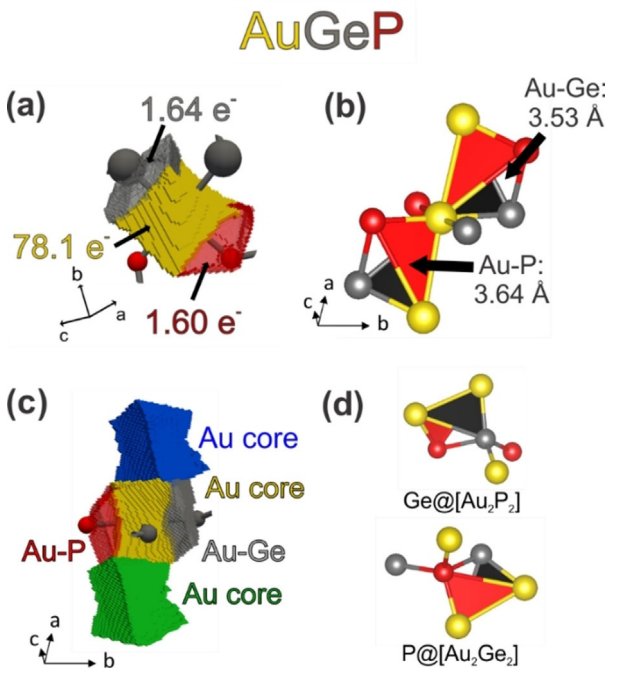

Figure 5. Basins assigned for a) a unit of square-planar $[AuGe_2P_2]$ with the Au core (yellow) basin, corresponding to a total of 78.1 e^- plotted with Au–Ge (gray) and Au–P (red) bonding basins with the respective integrations of electrons. b) Three-centered bond highlighted for Au–Ge–Au (black) and Au–P–Au (red) triangles based on chemical bonding analysis. c) The linear Au–Au–Au chain showing the Au–Ge (gray) basin directly touching two Au core basins (blue and yellow) and the Au–P (red) basin directly touching two Au core basins (yellow and green). d) Local tetrahedral coordination for Ge and P, with three-centered bonds highlighted (black and red triangles).

X-ray photoelectron spectroscopy (XPS)

To confirm the oxidation states of Au, XPS was conducted on cold-pressed pellets for four AuTtPn (Tt = Si, Ge; Pn = P, As) compounds. XPS spectra of as-prepared pellets were dominated by signals of oxidized Ge^{+4}, P^{+5}, $As^{+5/+3}$, and Si^{+4} components. It is quite common for as-prepared metals and semiconductors to have substantial oxidized components on the surface.[44,45] To remove oxidized species from the surface and reveal the electronic states of the bulk, the pellets were sputtered (up to 30 s). AuGeP is used as a representative dataset here (Figure 6) and similar results for AuSiP, AuSiAs, and AuGeAs can be found in Figure S9 in the Supporting Information. The oxidized Ge^{+4} and P^{+5} components observed at binding energies of 33.3 and 134.2 eV were significantly suppressed by sputtering, whereas signals from covalent Ge^0 (29.9 eV) and P^0 (129.5 eV) were not affected by sputtering, indicating that those are bulk signals. Similar binding energies were reported for covalent Ge and P in $GeAs_2$ and NiP_2.[16,44] The Au XPS spectrum also has two components. Before sputtering (at 0 s, top curve in Figure 6a), two sets of peaks, corre-

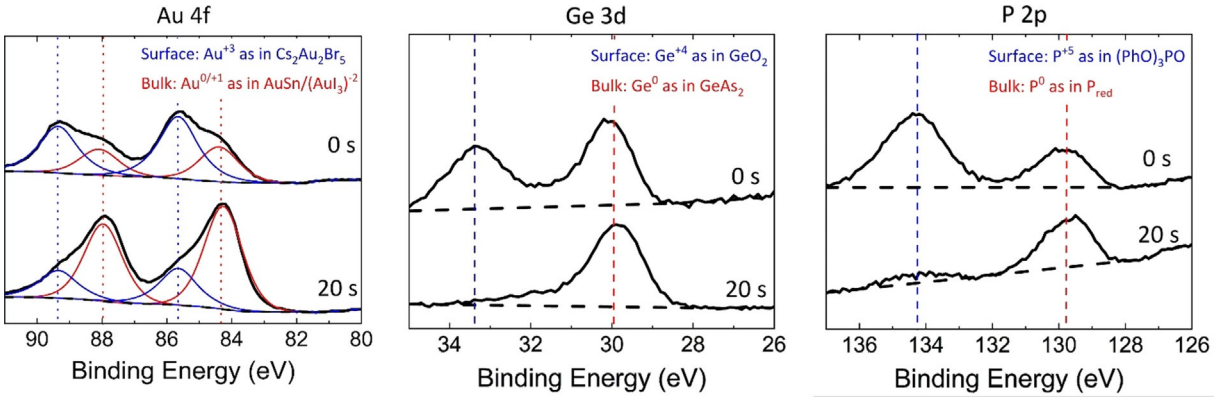

Figure 6. Au 4 f, Ge 3 d, and P 2 p XPS spectra for AuGeP before (0 s) and after (20 s) sputtering. Raw data (solid black line), background (black dashed line), and highlighted fit components (red and blue lines) for Au 4 f are shown. Vertical blue dashed lines indicate the signal corresponding to the oxidized surface species, which are reduced or removed after sputtering. Vertical red dashed lines indicate the signals corresponding to the bulk nature of the sample.

sponding to the Au 4 $f_{7/2}$ (84.2, 85.6 eV) and 4 $f_{5/2}$ (88.0, 89.3 eV) signals are observed. The higher energy peaks at 85.6 and 89.3 eV, shown in blue, decrease upon 20 s of sputtering. These signals seem to correspond to surface oxidation species of either Au^{III} as in cesium gold halides or partially ionic Au^{I} in molecular gold phosphine–chloride species.[44,46] The relative intensity of lower-energy Au signals (at 84.2 and 87.9 eV) increases after 20 s of sputtering, indicating that these correspond to bulk Au in the sample. The observed 4 $f_{7/2}$ binding energy for the bulk signal is similar to the energy of metallic gold (84 eV) or intermetallic AuSn and $AuSn_4$ (84.5–85 eV).[44] This shows that the conventional electron-counting scheme, in which Au would be expected to be in a +3 oxidation state, does not apply to the studied set of compounds. Instead, Au participates in covalent bonding with the 0/+1 oxidation state. Similar XPS Au signals are observed for covalent Au found in $Nd_{10}Au_3As_8O_{10}$, which exhibits [$AuAs_4$] square-planar units.[30]

Transport properties

Transport properties were measured on sintered pellets of AuGeP and AuSiAs with geometric densities of 72 and 62 %, respectively (Figure 7). The thermal conductivity was relatively low, 1.1–1.5 W mK^{-1}, at 300 K. The electronic contribution of the thermal conductivity was calculated by using the Wiedemann–Franz law and was estimated to be about 1 % of the total. Due to the low density of the studied pellets, the true thermal conductivity is expected to be higher. The thermal conductivity curve does not show a typical crystalline peak at lower temperatures (50–120 K). This shape is typical for amorphous materials that lack interfaces between crystallites, but it is also observed for crystalline materials, such as clathrates[47,48] and tetrahedrites.[49,50] AuGeP and AuSiAs exhibit *n*-type Seebeck coefficients, which are not common for complex pnictides, the majority of which are *p*-type materials,[51] although, *m*-NiP_2, which has a similar structure, also exhibits *n*-type behavior.[16] The difference observed from AuSiAs to AuGeP for both thermal conductivity and the Seebeck effect could be attributed to Ge/P mixing in AuGeP, a difference of pellet densities, and the overall trend of changing orbital overlap interactions. Thermal transport properties were not measured on AuGeAs, due to the inability to obtain a large pellet to attach TTO leads, only a four-probe electrical resistivity measurement was possible on a fragment of a pellet.

Electrical resistivity was measured for all three compounds (Figure 7). The resistivity of AuGeP and AuGeAs increases slightly with temperature, indicating semimetallic behavior. In turn, AuSiAs shows a weak decrease of resistivity with temperature, typical for heavily doped semiconductors. For AuGeP,

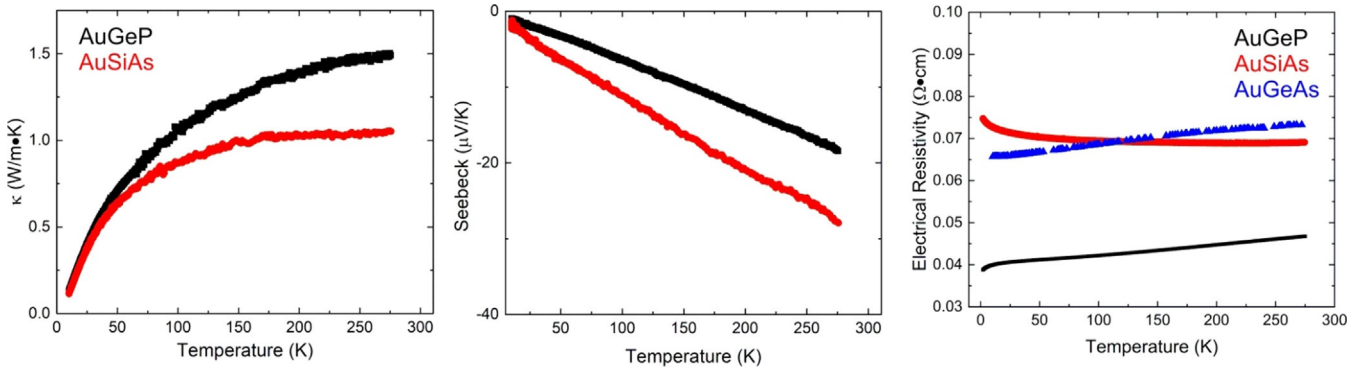

Figure 7. AuGeP (black), AuSiAs (red), and AuGeAs (blue) temperature-dependent transport properties measured from 10 to 280 K for thermal conductivity (left) and Seebeck effect (middle), and 2 to 280 K for electrical resistivity (right).

the antisite defects, for example, Ge/P substitutions, might be responsible for the semimetallic properties, which are different from the calculated narrow band gap semiconducting behavior. Similar Ge/As substitutions might take place for AuGeAs compounds, but those are difficult to detect. Finally, the AuSiAs compound with no antisite defects exhibits semiconductor-like behavior. Optical studies reveal that the experimental band gap of AuSiAs is lower than that of the instrument limit of 0.5 eV, indicating that the computed band gap of 0.7 eV is an overestimation. Overall, the novel phases were characterized as *n*-type semimetals/heavily doped semiconductors.

Conclusion

AuSiAs, AuGeP, and AuGeAs were discovered and characterized. The thermal stability decreases if Si is replaced with Ge or P with As. These phases all crystallize in the NCS space group *Cc* (no. 9), featuring square-planar Au within *cis*-[$AuTt_2Pn_2$], which is uncommon for extended solids. This is in drastic contrast to the structure of previously reported AuSiP, which exhibits a more common linear coordination of Au with Si and P. Chemical bonding analysis in direct space through the ELF suggests covalent two-center two-electron Tt–Pn bonds and three-center Au–Tt–Au and Au–Pn–Au bonds, with about 1.6 e^- per bond. For metal pnictides and tetrelides, this bonding is unconventional and stems from the high electronegativity of Au, which is the most electronegative element, despite being the metal in the studied compounds. XPS studies support the covalent, rather than ionic, nature of Au–Pn and Au–Tt bonds. The title materials were found to be *n*-type narrow-gap semiconductors or semimetals, with nearly temperature-independent electrical resistivities and low thermal conductivities. The combination of semimetallic properties with tunable NCS structures provides opportunities for the development of materials based on gold tetrel pnictides.

Experimental Section

Crystallographic data: Further details of the crystal structure investigations may be obtained from the joint CCDC/FIZ Karlsruhe online deposition service by quoting the deposition numbers CSD-204641, 2046416, and 2046417.

Acknowledgements

We would like to thank Professor Vitalij Pecharsky (Iowa State University and Ames Laboratory) for access to the arc-melting setup, and Professor Julia V. Zaikina and Adedoyin N. Adeyemi (Iowa State University) for access to SPS and the UV/Vis/NIR spectrometer. G.A. is grateful to the Ames Laboratory Spedding Postdoctoral Fellowship for financial support. This work was supported by the Ames Laboratory's Laboratory Directed Research and Development (LDRD) program (G.A., S.L., J.M., J.W., and K.K.) Ames Laboratory is operated for the US Department of Energy (DOE) by Iowa State University under contract no. DE-AC02-07CH11358. We would like to thank Dr. W. Xu and Dr. A. Yakovenko for help with conducting the in situ powder XRD measurements at 17-BM (APS-ANL). This research used resources of the Advanced Photon Source, a US DOE Office of Science User Facility operated for the DOE Office of Science by Argonne National Laboratory under contract no. DE-AC02-06CH11357.

Conflict of interest

The authors declare no conflict of interest.

Keywords: electron localization function · gold · noncentrosymmetric structures · tetrel pnictides · X-ray photoelectron spectroscopy

[1] P. Narang, C. A. C. Garcia, C. Felser, *Nat. Mater.* **2021**, *20*, 293 – 300.
[2] K. E. Woo, J. Wang, K. Wu, K. Lee, J.-A. Dolyniuk, S. Pan, K. Kovnir, *Adv. Funct. Mater.* **2018**, *28*, 1801589.
[3] J. Mark, J. Wang, K. Wu, J. G. Lo, S. Lee, K. Kovnir, *J. Am. Chem. Soc.* **2019**, *141*, 11976 – 11983.
[4] T. Yu, S. Wang, X. Zhang, C. Li, J. Qiao, N. Jia, B. Han, S.-Q. Xia, X. Tao, *Chem. Mater.* **2019**, *31*, 2010 – 2018.
[5] K. Zhong, C. Liu, M. Wang, J. Shi, B. Kang, Z. Yuan, J. Li, D. Xu, W. Shi, J. Yao, *Opt. Mater. Express* **2017**, *7*, 3571 – 3579.
[6] Inorganic Crystal Structure Database, ICSD, **2019**.
[7] P. Pyykkö, *Chemical Society Reviews* **2008**, *37*, 1967.
[8] L. Pauling, *The Nature of the Chemical Bond and the Structure of Molecules and Crystals: An Introduction to Modern Structural Chemistry*, Ithaca, N. Y.: Cornell University Press, **1960**.
[9] M. Jansen, *Chem. Soc. Rev.* **2008**, *37*, 1826 – 1835.
[10] M. Jansen, *Solid State Sci.* **2005**, *7*, 1464 – 1474.
[11] C. Corti, R. Holliday, *Gold: Science and Applications*, CRC Press, **2009**.
[12] M. C. Gimeno, in *Modern Supramolecular Gold Chemistry*, John Wiley & Sons, Ltd, **2009**, pp. 1 – 63.
[13] J. L. Zhang, S. Zhao, S. Sun, X. Lian, A. Tadich, D.-C. Qi, C. Gu, Z. Ma, Z. Li, W. Chen, *Chem. Mater.* **2020**, *32*, 8561 – 8566.
[14] P. Kaiser, W. Jeitschko, *Zeitschr. Naturforsch. B* **1997**, *52*, 462 – 468.
[15] E. Larsson, *Ark. Kemi* **1965**, *23*, 335 – 365.
[16] B. Owens-Baird, J. Xu, D. Y. Petrovykh, O. Bondarchuk, Y. Ziouani, N. González-Ballesteros, P. Yox, F. M. Sapountzi, H. Niemantsverdriet, Y. V. Kolen'ko, K. Kovnir, *Chem. Mater.* **2019**, *31*, 3407 – 3418.
[17] B. Owens-Baird, J. P. S. Sousa, Y. Ziouani, D. Y. Petrovykh, N. A. Zarkevich, D. D. Johnson, Y. V. Kolen'ko, K. Kovnir, *Chemical Science* **2020**, *11*, 5007 – 5016.
[18] R. Vincent, D. M. Bird, J. W. Steeds, *Philos. Mag. Part A* **1984**, *50*, 745 – 763.
[19] a) J. Mark, M. P. Hanrahan, K. E. Woo, S. Lee, A. J. Rossini, K. Kovnir, *Chem. Eur. J.* **2019**, *25*, 6392 – 6401; b) V. Weippert, T. Chau, K. Witthaut, L. Eisenburger, D. Johrendt, *Chem. Commun.* **2021**, *57*, 1332 – 1335.
[20] A. R. Eulenstein, D. Bogdanovski, H. Reinhardt, V. Miß, B. Roling, N. Hampp, R. Dronskowski, S. Dehnen, *Chem. Mater.* **2019**, *31*, 8839 – 8849.
[21] K. Lee, S. Kamali, T. Ericsson, M. Bellard, K. Kovnir, *Chem. Mater.* **2016**, *28*, 2776 – 2785.
[22] J. Mark, B. C. McBride, S. Lee, P. Yox, K. Kovnir, *ACS Appl. Energy Mater.* **2020**, *3*, 4168 – 4172.
[23] M. Khatun, A. Mar, *Zeitschr. Naturforsch. B* **2016**, *71*, 375 – 380.
[24] M. Khatun, S. S. Stoyko, A. Mar, *J. Solid State Chem.* **2016**, *238*, 229 – 235.
[25] V. Weippert, T. Chau, K. Witthaut, D. Johrendt, *Inorg. Chem.* **2020**, *59*, 15447 – 15453.
[26] Y. Park, M. G. Kanatzidis, *Inorg. Chem.* **2001**, *40*, 5913 – 5916.
[27] Y. Park, M. G. Kanatzidis, *J. Alloys Compd.* **1997**, *257*, 137 – 145.
[28] J. A. Kurzman, X. Ouyang, W. B. Im, J. Li, J. Hu, S. L. Scott, R. Seshadri, *Inorg. Chem.* **2010**, *49*, 4670 – 4680.
[29] G. C. B. Alexander, D. H. Fabini, R. Seshadri, M. G. Kanatzidis, *Inorg. Chem.* **2018**, *57*, 804 – 810.

[30] T. Bartsch, O. Niehaus, D. Johrendt, Y. Kobayashi, M. Seto, P. M. Abdala, M. Bartsch, H. Zacharias, R.-D. Hoffmann, B. Gerke, U. C. Rodewald, R. Pöttgen, *Dalton Trans.* **2015**, *44*, 5854 – 5866.
[31] F. Pan, L. Guggolz, F. Weigend, S. Dehnen, *Angew. Chem. Int. Ed.* **2020**, *59*, 16638 – 16643; *Angew. Chem.* **2020**, *132*, 16781 – 16786.
[32] U. Zachwieja, *Z. Anorg. Allg. Chem.* **1995**, *621*, 975 – 978.
[33] I. Zeiringer, N. Melnychenko-Koblyuk, A. Grytsiv, E. Bauer, G. Giester, P. Rogl, *J. Phase Equilib. Diffus.* **2011**, *32*, 115 – 127.
[34] W. Jeitschko, M. H. Möller, *Acta Crystallogr. Sect. B* **1979**, *35*, 573 – 579.
[35] J. Fulmer, D. C. Kaseman, J.-A. Dolyniuk, K. Lee, S. Sen, K. Kovnir, *Inorg. Chem.* **2013**, *52*, 7061 – 7067.
[36] J. Fulmer, O. I. Lebedev, V. V. Roddatis, D. C. Kaseman, S. Sen, J.-A. Dolyniuk, K. Lee, A. V. Olenev, K. Kovnir, *J. Am. Chem. Soc.* **2013**, *135*, 12313 – 12323.
[37] K. Lee, S. Synnestvedt, M. Bellard, K. Kovnir, *J. Solid State Chem.* **2015**, *224*, 62 – 70.
[38] Z. Tang, A. P. Litvinchuk, H.-G. Lee, A. M. Guloy, *Inorg. Chem.* **1998**, *37*, 4752 – 4753.
[39] H. Schmidbaur, A. Schier, *Chem. Soc. Rev.* **2012**, *41*, 370 – 412.
[40] W. Dörrscheidt, N. Niess, H. Schäfer, *Zeitschr. Naturforsch. B* **1976**, *31*, 890 – 891.
[41] T. Wadsten, S. Burmester, G. Cederberg, R. B. Jensen, C. T. Pederson, E. Larsen, *Acta Chem. Scand.* **1965**, *19*, 1232 – 1238.
[42] T. Wadsten, M. Vikan, C. Krohn, Å. Nilsson, H. Theorell, R. Blinc, S. Paušak, L. Ehrenberg, J. Dumanović, *Acta Chem. Scand.* **1967**, *21*, 593 – 594.
[43] J. P. Perdew, K. Burke, M. Ernzerhof, *Phys. Rev. Lett.* **1996**, *77*, 3865 – 3868.
[44] J. F. Moulder, *Handbook of X-Ray Photoelectron Spectroscopy: A Reference Book of Standard Spectra for Identification and Interpretation of XPS Data*, Physical Electronics Division, PerkinElmer Corporation, **1992**.
[45] J. V. Zaikina, T. Mori, K. Kovnir, D. Teschner, A. Senyshyn, U. Schwarz, Yu. Grin, A. V. Shevelkov, *Chem. Eur. J.* **2010**, *16*, 12582 – 12589.
[46] H. Kitagawa, N. Kojima, T. Nakajima, *J. Chem. Soc. Dalton Trans.* **1991**, 3121 – 3125.
[47] J.-A. Dolyniuk, B. Owens-Baird, J. Wang, J. V. Zaikina, K. Kovnir, *Materials Science and Engineering: R: Reports* **2016**, *108*, 1 – 46.
[48] T. Cox, V. Gvozdetskyi, M. Bertolami, S. Lee, K. Shipley, O. I. Lebedev, J. V. Zaikina, *Angew. Chem. Int. Ed.* **2021**, *60*, 415 – 423; *Angew. Chem.* **2021**, *133*, 419 – 427.
[49] D. I. Nasonova, V. Yu. Verchenko, A. A. Tsirlin, A. V. Shevelkov, *Chem. Mater.* **2016**, *28*, 6621 – 6627.
[50] Y. Xia, V. Ozoliņš, C. Wolverton, *Phys. Rev. Lett.* **2020**, *125*, 085901.
[51] K. Rajput, S. Baranets, S. Bobev, *Chem. Mater.* **2020**, *32*, 9616 – 9626.

Manuscript received: December 13, 2020
Accepted manuscript online: February 1, 2021
Version of record online: March 15, 2021